

1 **Electrically micro-polarized amorphous sodo-niobate film competing with crystalline**  
2 **lithium niobate second order optical response**

3  
4 *Lara Karam, Frédéric Adamietz, Dominique Michau, Claudia Gonçalves, Myungkoo Kang,*  
5 *Rashi Sharma, G. Senthil Murugan, Thierry Cardinal, Evelyn Fargin, Vincent Rodriguez,*  
6 *Kathleen A. Richardson, Marc Dussauze\**

7  
8 L. Karam, F. Adamietz, Prof. V. Rodriguez, Dr. M. Dussauze  
9 Institut des Sciences Moléculaires, UMR 5255 CNRS  
10 Université de Bordeaux  
11 351 Cours de la Libération, 33405, Talence Cedex, France  
12 E-mail : marc.dussauze@u-bordeaux.fr

13  
14 D. Michau, Dr. T. Cardinal, Prof. E. Fargin  
15 Institut de Chimie de la Matière Condensée de Bordeaux, UMR 5026 CNRS  
16 Université de Bordeaux  
17 87 avenue du Dr. Albert Schweitzer, 33600 Pessac Cedex, France

18  
19 Dr. C. Gonçalves, Dr. M. Kang, Dr. R. Sharma, Prof. K. A. Richardson  
20 CREOL, College of Optics and Photonics, Department of Materials Science and Engineering  
21 University of Central Florida  
22 Orlando, FL 32816, United States

23  
24 Dr. G. S. Murugan  
25 Optoelectronics Research Centre  
26 University of Southampton  
27 Southampton SO17 1BJ, United Kingdom

28  
29 Keywords: nonlinear optical materials, amorphous thin films, poling

30  
31 The design of active optical devices integrating second-order nonlinear (SONL) optical  
32 responses typically relies on the use of dielectric crystalline materials such as lithium niobate  
33 (LN) or semi-conductors such as GaAs. Despite high SONL susceptibilities, these materials  
34 present important geometry constrains inherent to their crystalline nature limiting the  
35 complexity of the designed photonic systems. Conversely, amorphous materials are versatile  
36 optical media compatible with broad platform designs possessing a wide range of optical  
37 properties attributable to their composition flexibility. Demonstrated here for the first time in  
38 an amorphous inorganic material, we report a magnitude of SONL optical susceptibility ( $\chi^{(2)}$   
39  $=29$  pm/V at  $1.06$   $\mu$ m) comparable to that of LN single crystal. By using a thermo-electrical  
40 imprinting process, fine control of the induced uniaxial anisotropy is demonstrated at the  
41 micrometer scale. This work paves the way for the future design of integrated nonlinear

42 photonic circuits based on amorphous inorganic materials enabled by the spatially selective  
43 and high SONL optical susceptibility of these promising and novel optical materials.  
44  
45  
46 Research efforts towards the realization of efficient integrated photonic circuits (IPCs) where  
47 active and passive optical components are combined on a single chip, have expanded over the  
48 past decade. While this technology continues to mature, there remains significant challenges  
49 associated with planar material optical function and multi-material integration. The design of  
50 complex photonic structures requires a spatial control at widely varying length scales (from  
51 micrometer to centimeter) and the merging of multiple optical and chemical functionalities  
52 (for sensing devices). A promising platform for IPCs is silicon based<sup>[1]</sup> due to the very high  
53 refractive index (RI) difference between the silicon waveguide and its cladding (air or silicon  
54 oxide) which induces strong confinement of light allowing unprecedented small bend radii  
55 (down to 1  $\mu\text{m}$ ); such attributes can thus minimize the resulting component's footprint.  
56 Thanks to this confinement, efficient third order optical processes like stimulated Raman  
57 scattering have been observed in silicon waveguides<sup>[1]</sup>. However, as many active optical  
58 devices rely on second order nonlinear (SONL) optical processes rather than third, silicon  
59 cannot meet this demand as it is centrosymmetric and thus possesses a  $\chi^{(2)}$  of zero. Efforts to  
60 modify this intrinsic behavior have been reported showing that one can break silicon's  
61 centrosymmetry and induce a  $\chi^{(2)}$  as high as 15 pm/V in a straight waveguide by depositing a  
62 straining layer on the waveguide's surface.<sup>[2]</sup> Another important platform for IPCs is lithium  
63 niobate (LN).<sup>[3]</sup> LN exhibits good optical transparency spanning from the visible to mid-  
64 infrared as well as a strong SONL response ( $\chi^{(2)}_{zzz}=55$  pm/V for the single crystal grown from  
65 the congruent melt)<sup>[4]</sup> making it a material of choice for active optical devices for  
66 telecommunication. Traditional approaches to form waveguides in bulk LN through processes

67 like  $\text{Ti}^+$  diffusion have been shown to result in low RI differences and thus don't allow for  
68 complex structures. Unlike silicon, LN crystal is not isotropic thus enabling a strong SONL  
69 optical response yet creating possible geometry restrictions in the realization of certain  
70 devices. Several methods can be used to circumvent this problem. One is to use LN thin films  
71 on insulators (LNOI) making possible the design of ridge and wire waveguides exhibiting  
72 appreciable RI difference.<sup>[3]</sup> Quasi-phase matching (QPM) for frequency conversion has been  
73 achieved on periodically grooved<sup>[5]</sup> dry etched or periodically poled<sup>[6]</sup> (based on domain  
74 inversion) LNOI waveguides with good results. Another strategy employed is to use the LN  
75 platform for its SONL optical properties but to rely on an easily patterned material to form the  
76 guiding structure. Amorphous materials are good candidates for this task. Electro-optical  
77 microring resonators and Mach-Zehnder interferometers have been realized on a LNOI  
78 platform with a patterned chalcogenide thin film waveguide.<sup>[7]</sup> Compared to their crystalline  
79 counterparts, amorphous materials are more flexible and versatile as they are compatible with  
80 a range of forming processes and their optical properties can be tailored by tuning their  
81 composition.

82 Since many active optical devices rely on SONL properties and since glass is isotropic, its use  
83 is often limited to passive components such as waveguides. It is well known that breaking the  
84 centrosymmetry of glass by heating the sample under a strong voltage followed by cooling  
85 back down before removal of the DC field (or thermal poling) can result in the formation of a  
86 stable SONL optical susceptibility at the glass' surface. This process was first observed in  
87 fused silica<sup>[8]</sup> and has since been extended to many different glass families including  
88 silicate,<sup>[9]</sup> heavy metal oxides,<sup>[10-12]</sup> chalcogenides<sup>[13]</sup> among others. It can also be applied to  
89 chromophores containing polymer<sup>[14-16]</sup>; hence, this constitutes a field of research beyond the  
90 scope of this paper but such applicability to multiple systems highlights the versatility of the  
91 approach. Thermal poling used as an imprinting process (employing a patterned electrode) has  
92 resulted in the demonstration of rigorous spatial control of a stable SONL susceptibility at the

93 micrometer scale in different bulk glasses.<sup>[17,18]</sup> To date, limited efforts to extend this effect to  
94 amorphous thin films suitable for integrated planar structures have been shown.<sup>[19–21]</sup> While  
95 interesting findings have resulted from these studies, no amorphous inorganic material (in  
96 bulk or thin film form) has to date exhibited SONL susceptibility levels of sufficient  
97 magnitude to replace LN-based structures.

98 This work describes the patterning of SONL susceptibility of amorphous thin film in the  
99 binary system  $\text{Nb}_2\text{O}_5\text{-Na}_2\text{O}$ , demonstrating its potential as a promising candidate system with  
100 a range of physical and optical properties suited to IPCs. To the best of our knowledge, only  
101 one other group has reported the RF sputtering synthesis of amorphous  $\text{NaNbO}_3$  thin films.<sup>[22]</sup>  
102 Here, we focus on one thin film composition containing 10 at.% of sodium with films  
103 prepared by radiofrequency (RF) sputtering. The cross section of these films as investigated  
104 by scanning electron microscopy (SEM) (**Figure 1a**) shows excellent thickness uniformity,  
105 good adhesion to the borosilicate microscope slide substrate with no evidence of  
106 delamination. The film appears homogenous at this scale, with no sign of porosity nor other  
107 microstructural defects which could lead to light scattering. The composition homogeneity  
108 throughout the thickness of the film has been confirmed by secondary ion mass spectroscopy  
109 (SIMS) measurements (**Figure 1b**) and the film's amorphous nature is validated by the x-ray  
110 diffraction (XRD) diffractogram (**Figure 1c**). The optical properties of the film are shown  
111 **Figure 1d** through **1f**. The film's refractive index dispersion has been quantified by two  
112 different techniques (ellipsometry and refractometry) and measurements from both are in  
113 good agreement; these data were successfully fitted using a Sellmeier equation<sup>[23]</sup> across a  
114 large spectral window (0.5 to 4.5  $\mu\text{m}$ ) where the film is transmissive. The film exhibits a  
115 refractive index of  $2.046 \pm 0.005$  at 1.064  $\mu\text{m}$  which is comparable to that reported for  
116 amorphous  $\text{Nb}_2\text{O}_5$ .<sup>[24]</sup> The transparency domain, reconstructed from transmission  
117 measurements in the visible and reflection measurements in the infrared due to the substrate's  
118 absorption (**Figure 1e** and **1f**), spans from 0.4 to 5  $\mu\text{m}$  exhibiting comparable optical

119 transparency to that shown by LN.<sup>[3]</sup> These measurements also confirm the absence of light  
120 scattering in the whole spectral region investigated, consistent with no evidence of  
121 nanocrystallinity in the film.

122 An efficient thermo-electrical imprinting process on ionic bulk glasses is characterized by a  
123 depletion of mobile cations under the conductive parts of the electrode. The next two figures  
124 clearly illustrate how this process is successfully transferred to amorphous thin films in the  
125 present work. The principle of the micro-poling treatment is illustrated in **Figure 2a**. Here, the  
126 electrode is comprised of an indium tin oxide (ITO) thin film that is ablated by laser  
127 irradiation to form alternating patterned regions of conductive and nonconductive zones. In a  
128 manner similar to that used in previous studies on bulk glasses,<sup>[17]</sup> Raman mapping (**Figure**  
129 **2b** through **2d**) of the band centered at  $850\text{ cm}^{-1}$  (Figure 2c) was used to track the sodium  
130 distribution on the surface of the patterned film. This band is attributed to Nb-O stretching  
131 modes where the oxygen is involved in an ionic bond with sodium. We observe a decrease of  
132 this band for regions of the thin film under the conductive zones of the electrode (zone 2)  
133 confirming the departure of sodium with the electrical field. Furthermore, a concurrent  
134 evolution of the signature associated with molecular oxygen (mapping of the band at  
135  $1550\text{ cm}^{-1}$ , Figure 2d) is seen, as observed in prior efforts where it was shown that this band is  
136 associated with an electronic or anionic conduction that compensates for the departure of  
137 positive charges.<sup>[25,26]</sup> Both maps show evidence of homogenous structural rearrangement of  
138 the film, corresponding to the regions of the electrode's pattern correlating and illustrating the  
139 spatial precision of the imprinting process. The localization, the geometry and the magnitude  
140 of the SONL optical response are discussed in **Figure 3**. Here, the second harmonic  
141 generation (SHG), evidence of the SONL optical response in the film, was probed under  
142 specular reflection conditions using a confocal microscope. The sample is oriented so that the  
143 linearly polarized incident light is perpendicular to the imprinted line (along the X axis, see  
144 Figure 2a for the orientation of the sample). The SHG signal is analyzed along the same

145 polarization orientation thus the term  $\chi^{(2)}_{xxx}$  of the SONL susceptibility tensor is probed. The  
146 SHG response is confined (c.f. **Figure 3a**) to regions where the sodium concentration gradient  
147 is the strongest (i.e. at the edge of the conductive part of the electrode). It is maximal at the  
148 border of the sodium-rich/sodium-depleted zones and decreases by three orders of magnitude  
149 over less than three microns.

150 The SHG response in the patterned domains is largest when the sample is oriented as  
151 described above (corresponding to 0 or 180° positions on the polar plot **Figure 3b**). When the  
152 orientation of the sample turns the signal gradually decays following a square cosine function  
153 to reach a complete extinction when the imprinted line is parallel to the incident light  
154 polarization (corresponding to 90 or 270 ° on the polar plot). This directional variation shows  
155 the uniaxial geometry of this response and the rigorous geometry control of the SONL  
156 susceptibility.

157 In order to quantify the magnitude of the SONL optical susceptibility obtained using our  
158 imprinting process on these sodo-niobate amorphous films, we have measured the SHG as a  
159 function of the incident power and compared it to that of a reference (**Figure 3c**). The  
160 reference material used is a bulk lithium niobate single crystal grown from a congruent melt.  
161 Both measurements were made under the exact same experimental conditions. Here, the  
162 incident and analyzed polarizations were along the bulk single crystal's c-axis so that only the  
163 strongest coefficient of the SONL susceptibility tensor of the crystalline reference  
164 ( $\chi^{(2)}_{zzz}=55\pm 6$  pm/V)<sup>[4]</sup> was probed. The SHG signal's quadratic dependence were fitted on the  
165 basis of the classical theoretical expression of the SHG intensity as a function of the incident  
166 power.<sup>[27]</sup> From these data, we extracted the magnitude of the thin film's SONL susceptibility  
167 using the ratio between the two quadratic law fitting coefficients, taking into account the  
168 different refractive indices, and incorporating a correction for the surface's reflection losses  
169 (all details are given in the supporting information). Employing this protocol, the SONL  
170 susceptibility micro-localized at the sodium-rich/sodium-depleted (on a scale of 3 μm)

171 frontier of these amorphous sodo-niobate films was determined to be  $29\pm 4$  pm/V. After  
172 demonstrating such accurate and spatially precise control of the second order optical  
173 properties for these electrically polarized amorphous optical thin films, the next step is  
174 naturally to progress toward the fabrication of features such as nonlinear optical amorphous  
175 waveguides which would be important geometries in the design of a planar optical devices.  
176 The lines that we have imprinted on the films are 5 mm long and a similar SHG response has  
177 been measured over their whole length ( $\pm 10$  % in intensity). Hence, we can reasonably  
178 prospect to apply this technique to induce a second order optical susceptibility over long  
179 distances which could be of interest for the design of an electro-optical waveguide. To  
180 achieve quasi phase patching conditions (QPM), a waveguide could be poled with a comb-  
181 like electrode (similar to the one used here<sup>[28]</sup>) on its side to obtain periodically alternating  
182 SONL active and non-active domains. Now, if a similar comb-like electrode were to be put on  
183 the other side of the waveguide but with a spatial offset, inverted domains could be formed  
184 along the waveguide. According to the index dispersion of these niobate amorphous films  
185 (Figure 1), the coherence length varies from 9 to 25  $\mu\text{m}$  for wavelengths ranging from 1.5 to 3  
186  $\mu\text{m}$ ; hence, the accuracy of the imprinting process demonstrated in this study denotes the  
187 feasibility to pattern the SONL properties of these niobate amorphous materials within this  
188 scale range.

189 In conclusion, we have synthesized and characterized the properties of amorphous sodo-  
190 niobate thin film materials. A thermo-electrical imprinting process was applied to these high  
191 optical quality thin films extending to thin films previously observed in bulk poling  
192 mechanisms. An unprecedented high SONL optical susceptibility for an amorphous inorganic  
193 material, on the order of magnitude of that of crystalline LN was demonstrated and quantified  
194 in side-by-side evaluation of both materials The fine control of the localization and the  
195 geometry of the resulting SONL response enabled through the use of patterned electrode, has  
196 demonstrated the potential viability of these materials in future devices. The fabrication

197 flexibility guaranteed by the amorphous nature of the sodo-niobate thin film combined with  
198 an easy protocol to induce microscale, local uniaxial anisotropies with  $\chi^{(2)}$  values, competing  
199 with a crystalline LN, opens vast new opportunities for the design and manufacturing of  
200 planar photonic architectures for the visible through mid-infrared spectral region.

201

### 202 **Experimental Section**

203 Detailed experimental procedures are reported in the Supporting Information.

204

### 205 **Supporting Information**

206 Supporting information is available from Wiley Online Library or from the author.

207

### 208 **Acknowledgments**

209 The authors would like to thank Mikhail Klimov, at the Material Characterization Facility  
210 (MCF) at UCF for conducting the SIMS measurements and Pieter Kik (CREOL) for giving  
211 access to his ellipsometer, Eric Lebraud, at the ICMCB common characterization service for  
212 carrying the XRD measurements. The authors also appreciate the helpful discussions with  
213 Juejun Hu at MIT for his relevant suggestions related to photonic device design constraints  
214 and requirements. The authors gratefully acknowledge the financial support of: IdEx  
215 Bordeaux (Cluster of Excellence LAPHIA and the allocated grant referred to as ANR-10-  
216 IDEX-03-03), the IdEx Bordeaux Visiting Scholar program, and the CNRS project  
217 EMERGENCE @INC2019. This project has received funding from the European Union's  
218 Horizon 202 research program under the Marie Skłodowska-Curie grant agreement No  
219 823941 (FUNGLASS).

220

### 221 **Competing Interests statements:**

222 The authors declare no competing interests.

223

224

225

Received:

226

Revised:

227

Published online:

228

### 229 **References**

230 [1] W. Bogaerts, P. De Heyn, T. Van Vaerenbergh, K. De Vos, S. Kumar Selvaraja, T.

231 Claes, P. Dumon, P. Bienstman, D. Van Thourhout, R. Baets, *Laser & Photon. Rev.*

232 **2012**, *6*, 47.

233 [2] R. S. Jacobsen, K. N. Andersen, P. I. Borel, J. Fage-Pedersen, L. H. Frandsen, O.

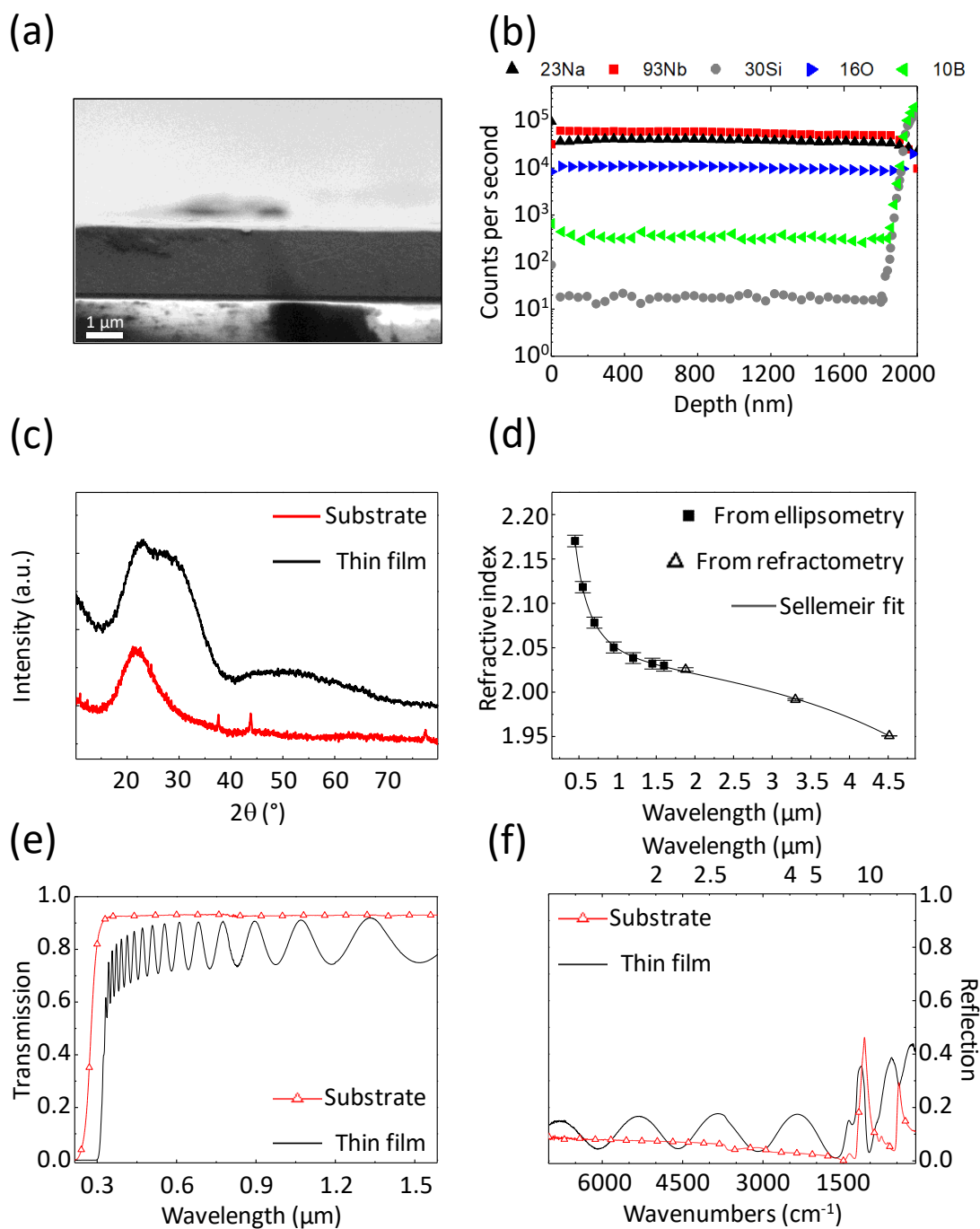
234 Hansen, M. Kristensen, A. V. Lavrinenko, G. Moulin, H. Ou, C. Peucheret, B. Zsigri, A.

235 Bjarklev, *Nature* **2006**, *441*, 199.

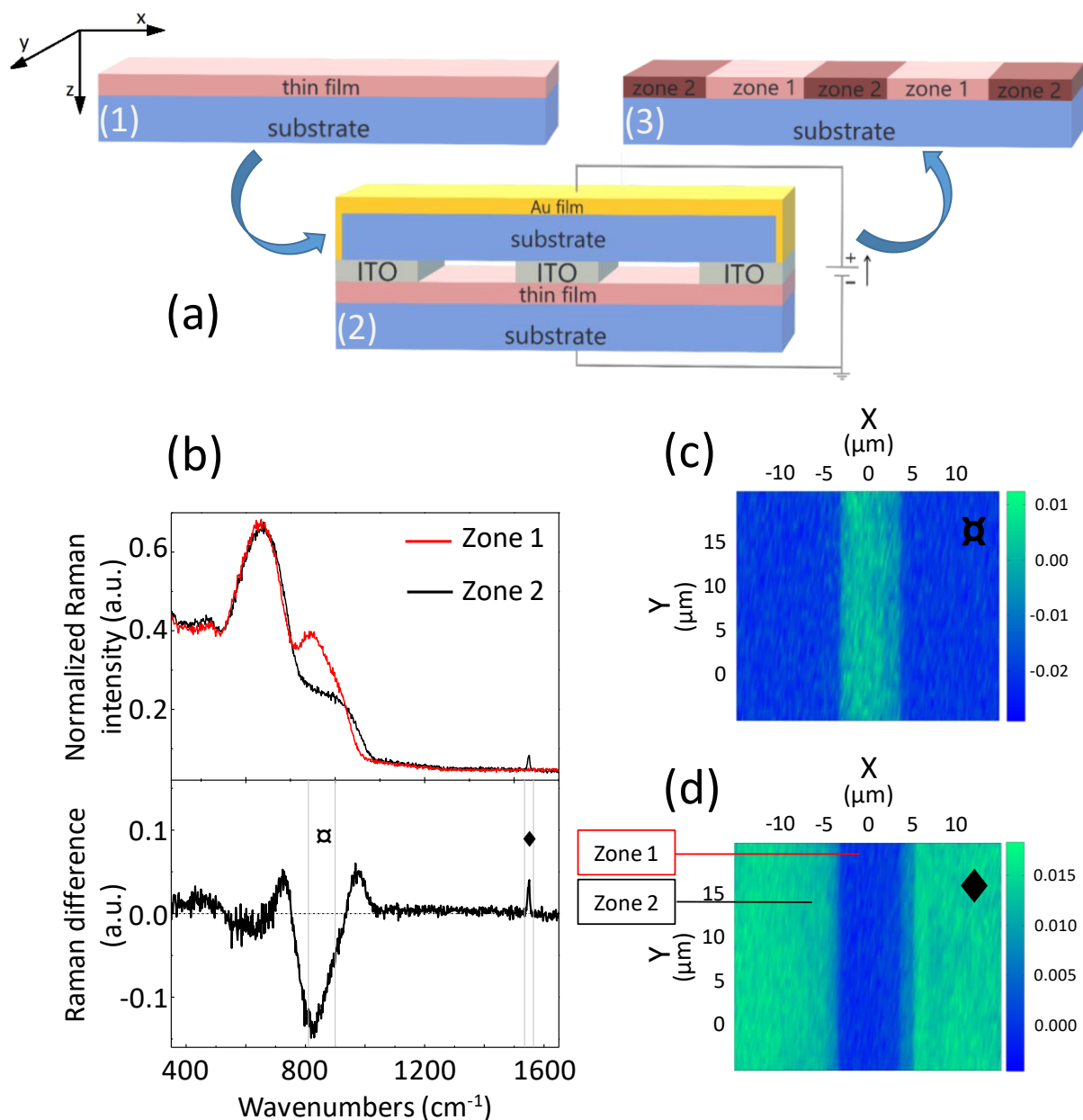


- 236 [3] A. Boes, B. Corcoran, L. Chang, J. Bowers, A. Mitchell, *Laser & Photonics Reviews*  
237 **2018**, *12*, 1700256.
- 238 [4] V. G. Dmitriev, G. G. Gurzadyan, D. N. Nikogosyan, *Handbook of Nonlinear Optical*  
239 *Crystals*, Springer Berlin Heidelberg, Berlin, Heidelberg, **1997**.
- 240 [5] C. Wang, X. Xiong, N. Andrade, V. Venkataraman, X.-F. Ren, G.-C. Guo, M. Lončar,  
241 *Opt. Express* **2017**, *25*, 6963.
- 242 [6] L. Chang, Y. Li, N. Volet, L. Wang, J. Peters, J. E. Bowers, *Optica* **2016**, *3*, 531.
- 243 [7] A. Rao, A. Patil, J. Chiles, M. Malinowski, S. Novak, K. Richardson, P. Rabiei, S.  
244 Fathpour, *Opt. Express* **2015**, *23*, 22746.
- 245 [8] R. A. Myers, N. Mukherjee, S. R. Brueck, *Optics Letters* **1991**, *16*, 1732.
- 246 [9] F. C. Garcia, I. C. S. Carvalho, E. Hering, W. Margulis, B. Lesche, *Applied Physics*  
247 *Letters* **1998**, *72*, 3252.
- 248 [10] B. Ferreira, E. Fargin, B. Guillaume, G. Le Flem, V. Rodriguez, M. Couzi, T. Buffeteau,  
249 L. Canioni, L. Sarger, G. Martinelli, Y. Quiquempois, H. Zeghlache, L. Carpentier,  
250 *Journal of Non-Crystalline Solids* **2003**, *332*, 207.
- 251 [11] K. Tanaka, A. Narazaki, K. Hirao, *Opt. Lett.* **2000**, *25*, 251.
- 252 [12] V. Nazabal, E. Fargin, J. J. Videau, G. Le Flem, A. Le Calvez, S. Montant, E. Freysz, A.  
253 Ducasse, M. Couzi, *Journal of Solid State Chemistry* **1997**, *133*, 529.
- 254 [13] M. Guignard, V. Nazabal, F. Smektala, J.-L. Adam, O. Bohnke, C. Duverger, A.  
255 Moréac, H. Zeghlache, A. Kudlinski, G. Martinelli, Y. Quiquempois, *Adv. Funct. Mater.*  
256 **2007**, *17*, 3284.
- 257 [14] S. K. Yesodha, C. K. Sadashiva Pillai, N. Tsutsumi, *Progress in Polymer Science* **2004**,  
258 *29*, 45.
- 259 [15] L. Dalton, in *Polymers for Photonics Applications I* (Ed.: K.-S. Lee), Springer Berlin  
260 Heidelberg, Berlin, Heidelberg, **2002**, pp. 1–86.

- 261 [16] P. Labbé, A. Donval, R. Hierle, E. Toussaere, J. Zyss, *Comptes Rendus Physique* **2002**,  
262 3, 543.
- 263 [17] M. Dussauze, V. Rodriguez, F. Adamietz, G. Yang, F. Bondu, A. Lopicard, M. Chafer,  
264 T. Cardinal, E. Fargin, *Advanced Optical Materials* **2016**, 4, 929.
- 265 [18] A. Lopicard, F. Adamietz, V. Rodriguez, K. Richardson, M. Dussauze, *Opt. Mater.*  
266 *Express* **2018**, 8, 1613.
- 267 [19] Y. Quiquempois, A. Villeneuve, D. Dam, K. Turcotte, J. Maier, G. Stegeman, S.  
268 Lacroix, *Electronics Letters* **2000**, 36, 733.
- 269 [20] M. Dussauze, A. Malakho, E. Fargin, J. P. Manaud, V. Rodriguez, F. Adamietz, B.  
270 Lazoryak, *Journal of Applied Physics* **2006**, 100, 013108.
- 271 [21] A. S. K. Tong, F. Bondu, G. Senthil Murugan, J. S. Wilkinson, M. Dussauze, *Journal of*  
272 *Applied Physics* **2019**, 125, 015104.
- 273 [22] V. Lingwal, N. S. Panwar, *Journal of Applied Physics* **2003**, 94, 4571.
- 274 [23] J. D. Musgraves, J. Hu, L. Calvez, *Springer Handbook of Glass*, **2019**.
- 275 [24] Ö. D. Coşkun, S. Demirel, G. Atak, *Journal of Alloys and Compounds* **2015**, 648, 994.
- 276 [25] T. Cremoux, M. Dussauze, E. Fargin, T. Cardinal, D. Talaga, F. Adamietz, V.  
277 Rodriguez, *The Journal of Physical Chemistry C* **2014**, 118, 3716.
- 278 [26] M. Dussauze, V. Rodriguez, A. Lipovskii, M. Petrov, C. Smith, K. Richardson, T.  
279 Cardinal, E. Fargin, E. I. Kamitsos, *J. Phys. Chem. C* **2010**, 114, 12754.
- 280 [27] R. W. Boyd, *Nonlinear Optics*, Elsevier, **2003**.
- 281 [28] P. Mackwitz, M. Rüsing, G. Berth, A. Widhalm, K. Müller, A. Zrenner, *Appl. Phys. Lett.*  
282 **2016**, 108, 152902.
- 283 [29] N. Bloembergen, P. S. Pershan, *Phys. Rev.* **1962**, 128, 606.

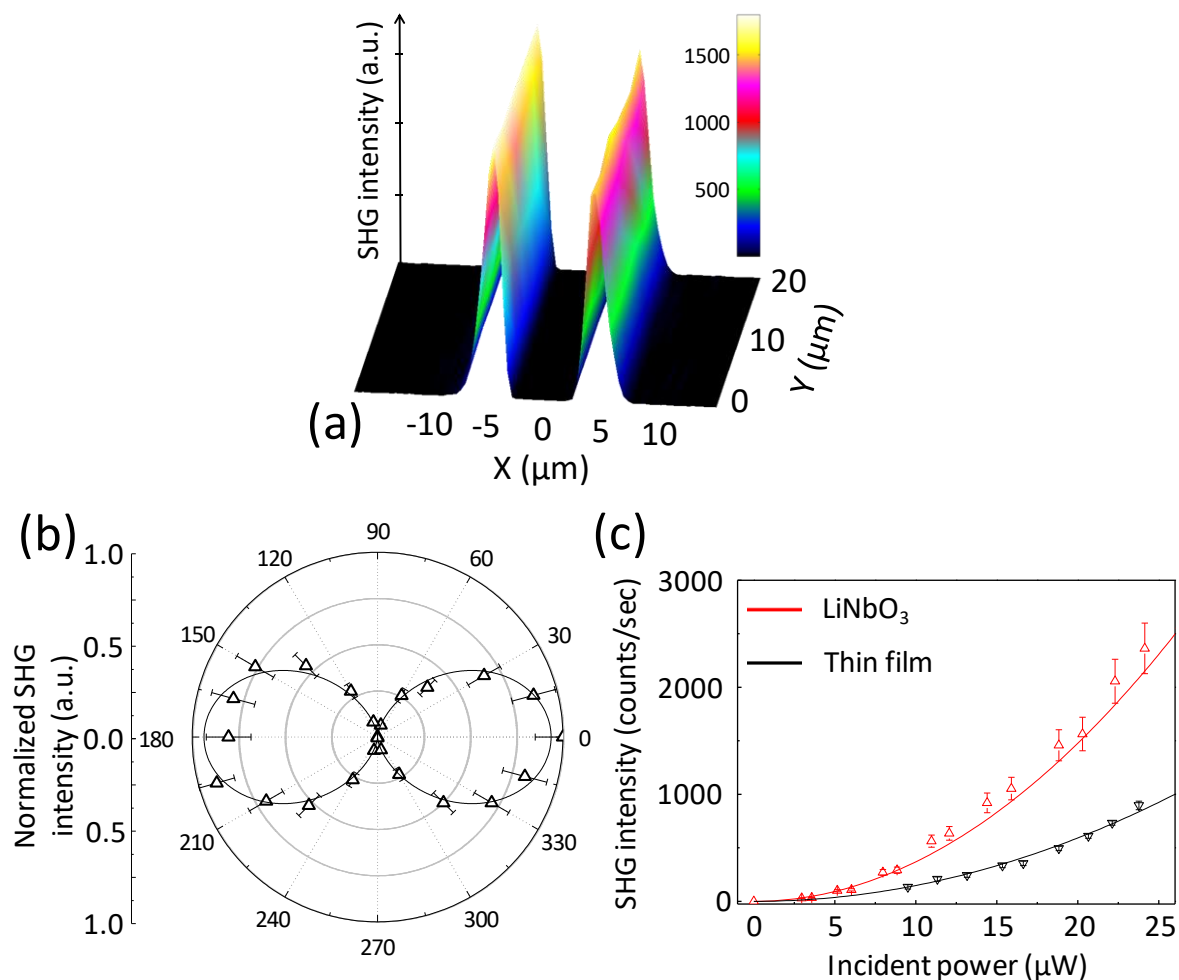


284  
 285 **Figure 1.** Characterization of the sodo-niobate film: a) Thin film on glass slide cross section  
 286 viewed by SEM, the scale bar is 1  $\mu\text{m}$ . b) SIMS profile recorded through the depth of the  
 287 film. Silicon and Boron concentration increase shows that the borosilicate glass substrate  
 288 interface was reached. c) XRD pattern of the bare borosilicate substrate (in red) and that of the  
 289 thin film (black) confirming the amorphous nature of both; the three peaks on the substrate's  
 290 diffractogram originate from the sample holder (aluminum). d) Film refractive index  
 291 dispersion obtained by a Sellmeier fit on data extracted from two different techniques; on the  
 292 refractometry measurements (opened squares) the error is within the size of the data point.  
 293 The transparency window of a 1.4  $\mu\text{m}$  thick film in black: transmission in the visible (e) and  
 294 reflection in the infra-red (f); as a comparison the substrate's spectra are also presented in red  
 295 (opened triangles).  
 296



297

298 **Figure 2.** Thermo-electrical micro-imprinting process: a) Schematic of the process: the sodio-  
 299 niobate thin film is deposited on a borosilicate glass slide (1), and heated while a strong  
 300 voltage is applied by a structured electrode (in contact with the sample as opposed to some  
 301 other techniques)<sup>[5]</sup> (2) and cooled back down before turning the DC field off. This gives rise to  
 302 two different zones on the post-processed sample (3). b) (top) The characteristic Raman  
 303 spectra (top) extracted from zone 1 (red) and 2 (black). The spectra have been normalized by  
 304 the area under the curve. To illustrate evidence of the structural variations of the two regions,  
 305 the difference Raman spectra is presented (bottom), corresponding to the response in zone 1  
 306 (unaffected by poling) subtracted to the poled region in zone 2. c), d) Spatial evolution of two  
 307 different bands: (c) corresponds Nb-O stretching modes associated with Nb-O...Na<sup>+</sup>  
 308 structural units, and (d) to spectral region illustrating the presence of molecular oxygen  
 309 attributed to compensation mechanisms occurring during poling.<sup>[17]</sup>



310

311 **Figure 3.** Localization, geometry and magnitude of the induced SONL optical response. a)  
 312 SHG intensity map realized on the poled film with a linearly polarized light (VV)  
 313 perpendicular to the imprinted line. b) Normalized SHG intensity as a function of the  
 314 orientation of the sample (0-180 ° corresponds to the imprinted line perpendicular to the  
 315 incident light polarization and 90-270 ° parallel). The data were normalized to the maximum  
 316 value. Repeating the experiment several times allows estimation of error bars to a value of  
 317 approximately 15 %. A fit with a  $\cos^2$  function demonstrates the uniaxial geometry of the  
 318 response. c) SHG intensity as a function of the linearly polarized incident light power for the  
 319 thin film (in black – oriented so that the imprinted line is perpendicular to the incident light)  
 320 and for the LN single crystal (in red – oriented so that the c axis is collinear to the incident  
 321 light polarization and so that  $\chi_{zzz}^{(2)}$  is probed). The error bar was estimated by repeating the  
 322 measurements. The continuous lines correspond to quadratic fits.  
 323

324 A second order nonlinear optical susceptibility is induced by a thermo-electrical imprinting  
325 treatment in an amorphous thin film. A magnitude for the  $\chi^{(2)}$  of 29 pm/V is measured, this  
326 value is the highest ever reported for an amorphous inorganic material. The induced uniaxial  
327 anisotropy is localized at the micrometer scale opening the way for new active planar  
328 photonic architectures based on amorphous materials.

329

### 330 Nonlinear Optical Materials

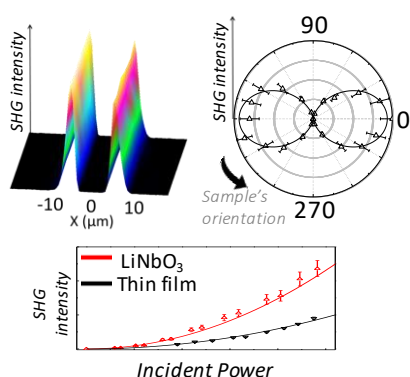
331

332 Lara Karam, Frédéric Adamietz, Dominique Michau, Claudia Gonçalves, Myungkoo Kang,  
333 Rashi Sharma, G. Senthil Murugan, Thierry Cardinal, Evelyn Fargin, Vincent Rodriguez,  
334 Kathleen A. Richardson, Marc Dussauze\*

335

336 **Electrically micro-polarized amorphous sodo-niobate film competing with crystalline**  
337 **lithium niobate second order optical response**

338



339

340